Transport properties of isospin asymmetric nuclear matter using the time-dependent Hartree-Fock method

A. S. Umar,[1] C. Simenel,[2] and W. Ye[3]
[1]*Department of Physics and Astronomy, Vanderbilt University, Nashville, Tennessee 37235, USA*
[2]*Department of Nuclear Physics, RSPE, Australian National University, Canberra, ACT 0200, Australia*
[3]*Department of Physics, Southeast University, Nanjing 210096, Jiangsu Province, People's Republic of China*
(Received 15 June 2017; published 30 August 2017)

Background: The study of deep-inelastic reactions of nuclei provides a vehicle to explore nuclear transport phenomena for a full range of equilibration dynamics. These investigations provide us the ingredients to model such phenomena and help answer important questions about the nuclear equation of state and its evolution as a function of neutron-to-proton (N/Z) ratio.
Purpose: The motivation is to examine the real-time dynamics of nuclear transport phenomena and its dependence on N/Z asymmetry from a microscopic point of view to avoid any pre-conceived assumptions about the involved processes.
Method: The time-dependent Hartree-Fock (TDHF) method in full three dimensions is employed to calculate deep-inelastic reactions of ^{78}Kr + ^{208}Pb and ^{92}Kr + ^{208}Pb systems at 8.5 MeV/nucleon. The impact parameter and energy-loss dependence of relevant observables are calculated. In addition, the density-constrained TDHF method is used to compute excitation energies of the primary fragments. The statistical deexcitation code GEMINI is utilized to examine the final reaction products.
Results: The kinetic energy loss and sticking times as a function of impact parameter are calculated. The final properties of the fragments (charge, mass, scattering angle, and kinetic energy) are computed. Their evolution as a function of energy loss is studied and various intra-relations are investigated. The fragment excitation energy sharing is computed.
Conclusions: We find a smooth dependence of the energy loss, $E_{\rm loss}$, on the impact parameter for both systems. However, the transfer properties for low $E_{\rm loss}$ values are very different for the two systems but become similar in the higher $E_{\rm loss}$ regime. The mean lifetime of the charge equilibration process, obtained from the final $(N-Z)/A$ value of the fragments, is shown to be ∼0.5 zs. This value is slightly larger than (but of the same order as) the value obtained from reactions at Fermi energies.

DOI: 10.1103/PhysRevC.96.024625

I. INTRODUCTION

Study of strongly damped collisions of nuclei or so called deep-inelastic collisions can play an important role in elucidating the dynamics of charge and mass exchange, dissipation of energy and angular momentum, degree of isospin equilibration, and the dependence of these quantities on the properties of the reactants such as the neutron-to-proton ratio (N/Z) [1–3]. In addition, these reactions probe an intriguing interplay between the microscopic single-particle dynamics and collective motion at time scales too short for full equilibration. For these collisions Coulomb and centrifugal interactions overcome the strong nuclear attraction and result in final fragments somewhat reminiscent of the initial projectile and target and thus occupy the regime between quasielastic and fusion-fission reactions. It has also been suggested to use deep-inelastic reactions for isotope production [4].

One of the major open questions in strongly damped reactions is the dependence of the final state products (and related observables) on the neutron excess, or equivalently on the total isospin quantum number $T_z = (Z-N)/2$. Besides being a fundamental nuclear structure and reaction question, the answer to this inquiry is also vital to our understanding of the nuclear equation of state (EOS) and symmetry energy [5–9]. The EOS plays a key role in elucidating the structure of exotic nuclei [10,11], the dynamics of heavy-ion collisions [5,12], the composition of neutron stars [13], and the mechanism of core-collapse supernovae [14].

Transport properties of isospin asymmetric nuclear matter can be investigated by studying charge equilibration driven by the nuclear symmetry energy in heavy-ion collisions. For example, collisions at Fermi energies give access to contact times which are short enough to induce only a partial charge equilibration [15] and thus can be used to determine equilibration times [16]. Alternatively, charge equilibration has also been studied with deep-inelastic collisions at lower energies, but with large isospin asymmetry in the entrance channel [17–19]. To reveal possible systematic trends requires both theoretical and experimental studies with a wide variety of projectile and target combinations which are expected to become available at current and future radioactive ion-beam (RIB) facilities [20]. In addition, the much greater degree of isospin asymmetry available with RIBs will allow timescale and degree of isospin equilibration to be studied in detail [15]. In recent years a number of transport models have been employed to investigate the density dependence of the symmetry energy away from the saturation density [5,21–26]. While considerable success has been achieved in

obtaining information about the EOS from these calculations more refinement of the models is needed to make a deeper connection to fundamental aspects of nuclear many-body physics.

Deep-inelastic reactions at lower energies ($E \lesssim 20$ MeV/nucleon) have been historically studied using statistical nucleon transport models [27–29].

Many studies have concluded that one-body dissipation [30,31] and friction models [32,33] coupled with the proper choice of collective coordinates provide a reasonable approach to study these reactions. However, difficulties exist in modeling these reactions due to their time-dependent nonequilibrium nature. The portioning of excitation energy between the final fragments [3,34–36], the amount of irreversible energy dissipation as opposed to excitation of collective modes, the conversion of angular momentum to intrinsic spins of the final fragments [37], and the influence of transfer [33,38,39] have all been subject to experimental [18,40–42] scrutiny with often less than satisfactory comparisons [3,43]. Part of the complication arises from the model dependence of the experimental analysis. For example, determination of excitation energies requires the modeling of the decay or fission of the primary fragments. Recently, new experiments with RIBs have been proposed to elucidate some of these discrepancies [44]. These, coupled with theoretical studies that are microscopic and dynamical in nature, can further our understanding of the dependence of these reactions on the N/Z asymmetry and the shell structure of the participating nuclei.

For these low-energy heavy-ion collisions the relative motion of the centers of the two nuclei is characterized by a short wavelength and thus allows for a classical treatment, whereas the wavelength for the particle motion is not small compared to nuclear sizes and should be treated quantum mechanically [45]. The mean-field approach such as the time-dependent Hartree-Fock (TDHF) theory provides a microscopic basis for describing the heavy-ion reaction mechanism at low bombarding energies [46–48]. TDHF collisions which result in well separated final fragments provide a means to study the deep-inelastic scattering of heavy systems, allowing for the calculation of certain scattering observables, such as the final mass, charge, and scattering angles of the fragments. These are simply calculated by taking expectation values of one-body operators. The final scattering angles are found by matching the outgoing channel after separation to a pure Coulomb trajectory [49].

Owing to numerical complexity and the demand of extensive computer time the early TDHF calculations of deep-inelastic collisions employed approximations and assumptions that were not present in the basic theory, such as the limitation to an approximate two-dimensional collision geometry and the use of the rotating frame approximation, less accurate lattice discretization techniques, and less accurate energy-density functionals without the spin-orbit interaction [49,50]. Approximations of this type limit the number of degrees of freedom accessible during a collision and hence the nature and degree of dissipation. Subsequently, the relaxation of these approximations [51,52] has been shown to remedy many of the earlier shortcomings [53]. In addition, one-body energy dissipation extracted from TDHF calculations for low-energy fusion reactions was found to be in agreement with the friction coefficients based on the linear response theory as well as those in models where the dissipation was specifically adjusted to describe experiments [54]. All of these new results suggest that TDHF dynamics provides a good description of heavy-ion collisions. However, in the mean-field approximation since the collective aspects of the collision dynamics are treated semiclassically the fluctuations of the macroscopic variables are severely inhibited. To remedy this problem one must go beyond the TDHF approach [55–57].

Recent TDHF studies have been performed to investigate the charge equilibration in deep-inelastic collisions [56,58,59] and its impact on the interplay between fusion and transfer reactions [60–65]. Recent investigations have also shown that the one-body dissipation mechanisms included in the TDHF studies were the most relevant to describe fully damped reactions such as quasifission [66–71]. In this paper we study various aspects of deep-inelastic collisions using the TDHF approach. To examine the effects of N/Z asymmetry we chose the systems ^{78}Kr + ^{208}Pb and ^{92}Kr + ^{208}Pb. (Intense beams of neutron-rich ^{92}Kr will be available at future RIB facilities). The excitation energy of the primary fragments is calculated using the density-constrained TDHF (DC-TDHF) approach [72,73]. We also utilize the GEMINI code to study the decay of the primary fragments. In the next section we give an outline of the theoretical methods employed. This is followed by the results in Sec. III. We conclude by giving a summary of findings and future prospects in Sec. IV.

II. THEORETICAL OUTLINE

A. Time-dependent Hartree-Fock method

The TDHF theory is a mean-field approximation of the exact time-dependent many-body problem. Formally, the strong repulsion between nucleons at short distances requires a rearrangement of the standard perturbation theory leading to the suppression of the strong N-N interaction terms and resulting in an effective two-body interaction. The equations of motion governing the nuclear system are derived using the time-dependent variational principle and lead to the replacement of the original linear quantum mechanics by a set of coupled nonlinear equations. The resulting mean-field approximation yields an excellent description of nuclei throughout the periodic table and has been successful in the description of the inclusive properties of low-energy heavy-ion collisions. Generally, heavy-ion collisions at energies of a few MeV per nucleon above the Coulomb barrier are either predominantly fusion or predominantly deep-inelastic reactions. In both cases we are in a regime where classical descriptions of the relative motion are approximately valid. Thus, TDHF simulations of these collisions with definite impact parameters are expected to yield quantitatively good agreement with the corresponding experimental data. While the TDHF approach provides a good starting point for a fully microscopic theory of large amplitude collective motion [46–48], only in recent years has it become feasible to perform TDHF calculations on a three-dimensional Cartesian grid

without any symmetry restrictions and with accurate numerical methods [74–81]. In addition, the quality of energy-density functionals has been substantially improved [82–84].

Given a many-body Hamiltonian $\hat{H}$, the action S can be constructed as

$$S = \int_{t_1}^{t_2} dt \langle \Phi(t)|\hat{H} - i\hbar\partial_t|\Phi(t)\rangle. \quad (1)$$

Here, Φ denotes the time-dependent correlated many-body wave function, $\Phi(\mathbf{r_1},\mathbf{r_2},\ldots,\mathbf{r_A};t)$. The variational principle $\delta S = 0$ is then equivalent to the time-dependent Schrödinger equation. In the TDHF approximation the many-body wave function is replaced by a single Slater determinant and this form is preserved at all times. The determinantal form guarantees the antisymmetry required by the Pauli principle for a system of fermions. In this limit, the variation of the action yields the most probable time-dependent mean-field path between points t_1 and t_2 in the multi-dimensional space-time phase space:

$$\delta S = 0 \rightarrow \Phi_0(t), \quad (2)$$

where $\Phi_0(t)$ is a Slater determinant with the associated single-particle states $\phi_\lambda(\mathbf{r},t)$. The variation in Eq. (2) is performed with respect to the single-particle states ϕ_λ and ϕ^*_λ. This leads to a set of coupled, nonlinear, self-consistent initial value equations for the single-particle states,

$$h(\{\phi_\mu\})\phi_\lambda = i\hbar\partial_t\phi_\lambda, \quad \lambda = 1,\ldots,N, \quad (3)$$

and their Hermitian conjugates, where N is the number of particles. These are the fully microscopic TDHF equations. As we see from Eq. (3), each single-particle state evolves in the mean field generated by the concerted action of all the other single-particle states.

In standard TDHF applications to heavy-ion collisions, the initial nuclei are calculated using the static Hartree-Fock (HF) theory and the Skyrme functional [82]. The resulting Slater determinants for each nucleus comprise the larger Slater determinant describing the colliding system during the TDHF evolution. Nuclei are assumed to move on a pure Coulomb trajectory until the initial separation between the nuclear centers used as the initial condition in the TDHF evolution. Of course, no assumption is made on the subsequent trajectory in the TDHF evolution. Using the Coulomb trajectory we compute the relative kinetic energy at this separation and the associated translational momenta for each nucleus. The nuclei are then boosted by multiplying the HF states with

$$\Phi_j \rightarrow \exp(\imath\mathbf{k}_j\cdot\mathbf{R})\Phi_j, \quad (4)$$

where Φ_j is the HF state for nucleus j and $\mathbf{R}$ is the corresponding center of mass coordinate:

$$\mathbf{R} = \frac{1}{A_j}\sum_{i=1}^{A_j}\mathbf{r}_i. \quad (5)$$

The Galilean invariance and the conservation of the total energy in the Skyrme TDHF equations are used to check the convergence of the calculations.

Since TDHF is based on the independent-particle approximation it can be interpreted as the semiclassical limit of a fully quantal theory thus allowing a connection to macroscopic coordinates and providing insight about the collision process. In this sense the TDHF dynamics can only be used to compute the semiclassical trajectories of the collective moments of the composite system as a function of time. Note that the part of the residual interaction that is neglected in the TDHF approach may produce fluctuations and correlations that affect these trajectories. Recent developments beyond the TDHF approach have been used to investigate the effects of such fluctuations in heavy-ion collisions [56,85]. However, the TDHF approach is optimized to the expectation values of one-body operators [86] and is then capable to predict these quantities. This was demonstrated by the recent successes of the TDHF approach in reproducing various reaction mechanisms in heavy-ion collisions. Moreover, beyond-TDHF calculations remain numerically difficult. We then restrict the present calculations to the TDHF level.

B. DC-TDHF method and excitation energies

The excitation energy and, in particular, its repartition between the fragments also provide important information on the dissipative nature of the reaction mechanisms [3,87]. In the TDHF approach, thermalization is only partial as it only contains one-body dissipation mechanisms such as nucleon evaporation [88,89] and damping of collective energy with (nearly) random collisions of nucleons with the walls of the mean field. One-body energy dissipation extracted from TDHF calculations for low-energy fusion reactions was also found to be in agreement with the friction coefficients based on the linear response theory as well as those in models where the dissipation was specifically adjusted to describe experiments [54].

Based on the strategy proposed in Ref. [90], we recently developed an extension to TDHF theory via the use of a density constraint to calculate the fragment excitation energy of *each fragment* directly from the TDHF time evolution [72]. For this purpose, we divide the conserved TDHF energy into a collective and intrinsic part, and we assume that the collective part is primarily determined by the density $\rho(\mathbf{r},t)$ and the current $\mathbf{j}(\mathbf{r},t)$. Consequently, the excitation energy can be written in the form

$$E^*(t) = E_{\rm TDHF} - E_{\rm coll}(\rho(t),\mathbf{j}(t)), \quad (6)$$

where $E_{\rm TDHF}$ is the total energy of the dynamical system, which is a conserved quantity, and $E_{\rm coll}$ represents the collective energy of the system. The collective energy consists of two parts,

$$E_{\rm coll}(t) = E_{\rm kin}(\rho(t),\mathbf{j}(t)) + E_{\rm DC}(\rho(t)), \quad (7)$$

where $E_{\rm kin}$ represents the kinetic part and is given by

$$E_{\rm kin}(\rho(t),\mathbf{j}(t)) = \frac{m}{2}\int d^3r\ \mathbf{j}^2(t)/\rho(t), \quad (8)$$

which is asymptotically equivalent to the kinetic energy of the relative motion, $\frac{1}{2}\mu\dot{R}^2$, where μ is the reduced mass and $R(t)$ is the ion-ion separation distance. The energy $E_{\rm DC}$ is the density-constrained TDHF energy, the lowest-energy state of all possible TDHF states with the same density with

no excitation [91]. This gives us new information on the repartition of the excitation energy between the heavy and light fragments which is not available in standard TDHF calculations, except with projection techniques [92].

III. RESULTS

We used TDHF theory to study the reactions ^{78}Kr + ^{208}Pb and ^{92}Kr + ^{208}Pb at the energy $E = 8.5$ MeV/nucleon. TDHF calculations were done in a numerical Cartesian box which is 65 fm along the collision axis, 50 fm in the reaction plane perpendicular to the reaction axis, and 30 fm in the direction perpendicular to the reaction plane. The two nuclei are placed at an initial separation of 30 fm. Calculations used the SLY4D Skyrme functional [76] without the pairing interaction as described in Ref. [79]. Static calculations are done using the damped-relaxation method [93]. Krypton nuclei used in these calculations are deformed with deformation parameters $\beta_2 = 0.088$ for ^{78}Kr and $\beta_2 = 0.178$ for ^{92}Kr. To account for this deformation dependence we performed two sets of calculations for each Kr nucleus, one with the symmetry axis of the nucleus in the direction of the collision axis ($\beta = 0^\circ$) and the other with the symmetry axis perpendicular the collision axis ($\beta = 90^\circ$).

A. Main scattering features

In Fig. 1 we plot the ratio of the kinetic energy loss to the center-of-mass (c.m.) energy, $E_{\rm loss}/E_{\rm c.m.}$, versus impact parameter b (in femtometers) for both reactions. Energy loss is defined as the difference in initial c.m. energy and final c.m. energy of the outgoing fragments. The angle β represents the initial orientation of the deformed Kr nucleus with respect to the beam axis as discussed above. We note that for both systems there is a plateau for the energy loss for impact parameters up to about $b = 6$ fm. For larger impact parameters energy loss gradually decreases as expected. We also note that the energy loss for the neutron-rich ^{92}K reaction is considerably larger than the one for the ^{78}Kr collision. This can be interpreted as an effect of the higher beam energy in the ^{92}Kr + ^{208}Pb reaction. (Both reactions have the same beam energy of 8.5 MeV/nucleon, but ^{92}Kr is ∼15% heavier and thereby more energetic than ^{78}Kr.) Another interesting point is that the initial orientation of the Kr nuclei seems to have a minimal effect on the energy loss for the reaction. Figures 2 and 3 show the numbers of neutrons and protons transferred to and from the projectilelike fragment (PLF) for the reactions ^{78}Kr + ^{208}Pb and ^{92}Kr + ^{208}Pb, respectively. As anticipated for small energy losses originating from larger impact parameters the transfer of nucleons diminishes. However, for larger energy losses we notice important differences between the two systems. In the case of the ^{78}Kr + ^{208}Pb system, neutron transfer to the PLF gradually increases with increasing energy loss and peak around 50% $E_{\rm loss}/E_{\rm c.m.}$. At this energy loss, corresponding to the plateau region of Fig. 1, we see a large range of 4–15 neutrons transferred to the PLF. An important point to notice is that the transfer is unidirectional, namely, to the PLF only. The orientation effects of the ^{78}Kr are more pronounced with the $\beta = 90^\circ$ orientation resulting in larger transfers at the maximum energy loss. The situation for proton transfer is more complicated than that for neutrons. For small energy losses the protons seem to be transferred from ^{78}Kr to ^{208}Pb for up to about 42% $E_{\rm loss}/E_{\rm c.m.}$, subsequently changing

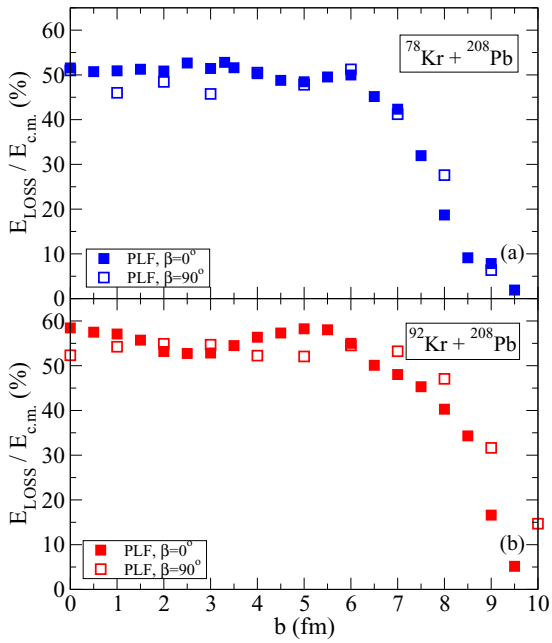

FIG. 1. Energy loss, $E_{\rm loss}/E_{\rm c.m.}$, versus impact parameter b (fm) for the reactions (a) ^{78}Kr + ^{208}Pb and (b) ^{92}Kr + ^{208}Pb at $E = 8.5$ MeV/nucleon. Angle β represents the initial orientation of the deformed ^{78}Kr nucleus with respect to the beam axis.

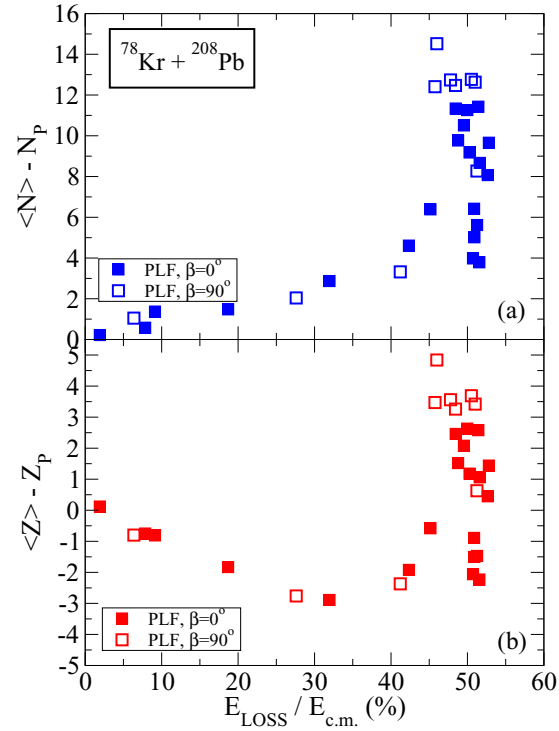

FIG. 2. (a) Neutron and (b) proton numbers transferred to and from the PLF for the reaction ^{78}Kr + ^{208}Pb at $E = 8.5$ MeV/nucleon as a function of $E_{\rm loss}/E_{\rm c.m.}$. Angle β represents the initial orientation of the deformed ^{78}Kr nucleus with respect to the beam axis.

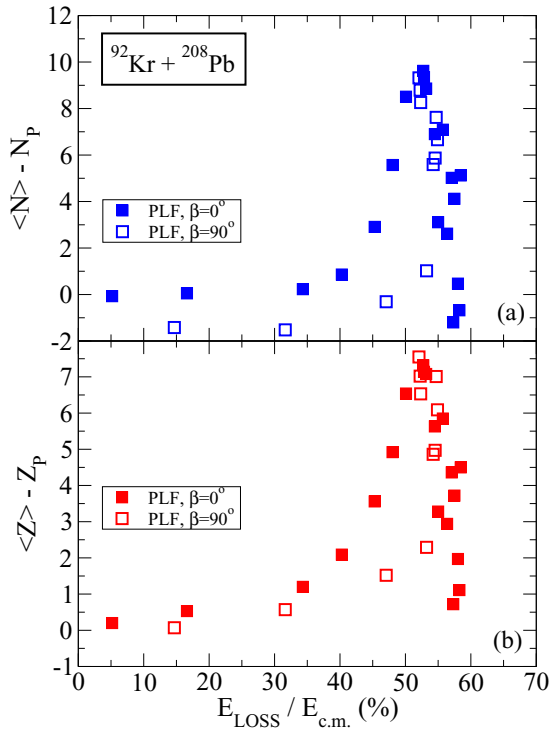

FIG. 3. (a) Neutron and (b) proton numbers transferred to and from the PLF for the reaction ^{92}Kr + ^{208}Pb at $E = 8.5$ MeV/nucleon as a function of $E_{\rm loss}/E_{\rm c.m.}$. Angle β represents the initial orientation of the deformed ^{92}Kr nucleus with respect to the beam axis.

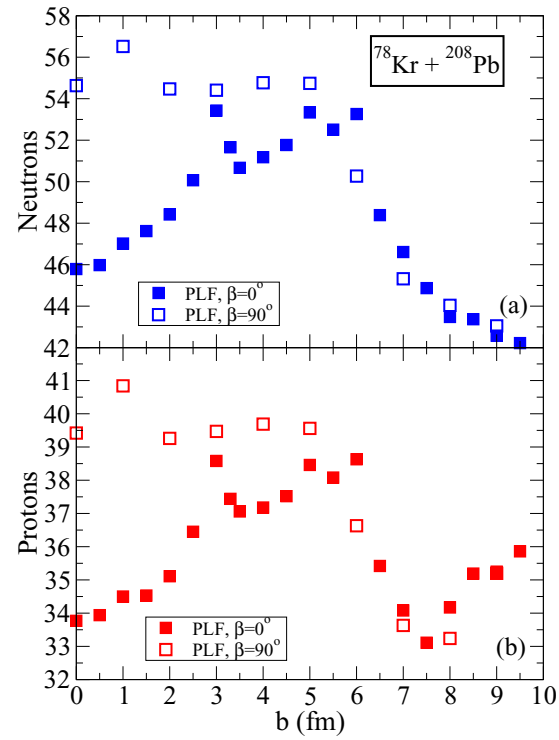

FIG. 4. (a) Neutron and (b) proton numbers of the PLF for the reaction ^{78}Kr + ^{208}Pb at $E = 8.5$ MeV/nucleon as a function of impact parameter b (fm). Angle β represents the initial orientation of the deformed ^{78}Kr nucleus with respect to the beam axis.

direction. At the maximum-energy-loss region the transfers for the $\beta = 90^\circ$ orientation is from ^{208}Pb to ^{78}Kr, whereas the $\beta = 0^\circ$ orientation results in transfers in both directions. One may understand this behavior in terms of N/Z equilibration as follows: For small energy losses and small transfers the neutron-poor ^{78}Kr nucleus can equilibrate faster by giving away some protons and receiving a small number of neutrons. However, as it receives more and more neutrons it no longer has to give out protons and actually now it can receive some protons. A more detailed discussion about the behavior in the maximum-energy-loss region is given below. Figure 3 shows the neutron and proton transfers to and from the PLF for the ^{92}Kr + ^{208}Pb system. In this case most of the neutron and all of the proton transfer is from ^{208}Pb to ^{92}Kr. Only for the $\beta = 90^\circ$ orientation of ^{92}Kr we see a region of energy loss where a few neutrons are transferred in the opposite direction. In the region of small energy loss we see no appreciable neutron transfer to the PLF while a small proton transfer takes place. For larger energy losses the number of transferred protons increases followed by the transfer of neutrons. Around the maximum energy loss corresponding to 52% of $E_{\rm loss}/E_{\rm c.m.}$, a wide distribution of transfers occur. Again, this behavior can largely be explained as a dynamical N/Z equilibration.

To gain more insight about the dependence of transfer on reaction dynamics we can investigate the impact parameter dependence of these reactions. In Fig. 4 we plot the neutron and proton numbers of the PLF for the reaction ^{78}Kr + ^{208}Pb at $E = 8.5$ MeV/nucleon as a function of impact parameter. Here, the dependence of transfer on the Kr orientation angle β is much more pronounced. While for larger impact parameters ($b > 6$ fm) the dependence on orientation is negligible, for smaller impact parameters we observe much larger neutron and proton transfer for the $\beta = 90^\circ$ orientation of ^{78}Kr. As a matter of fact for central impact parameters ($b < 3$ fm) the transfer of protons to PLFs occurs in opposite directions for the two orientations. For these impact parameters the $\beta = 90^\circ$ orientation has large neutron and proton transfers to the PLF, whereas the $\beta = 0^\circ$ orientation actually loses protons and gains a few neutrons. For large impact parameters ($b > 6$ fm) there is proton transfer from ^{78}Kr, which reaches a maximum at $b = 7.5$ fm. The corresponding plot of neutron and proton numbers of the PLF for the ^{92}Kr + ^{208}Pb system is shown in Fig. 5. For this system, for central impact parameters, we see an increase in transfer as the impact parameter increases for both orientations. Subsequently, for the $\beta = 0^\circ$ orientation there is a drop in both the neutron and proton curves around $b = 4.5$ fm, practically going down to no transfer. In contrast, transfer for the $\beta = 90^\circ$ orientation remains high in this region. For larger impact parameters, transfer for both orientations decreases gradually. One can characterize the structures seen in the impact parameter dependence as being comprised of fine structures and gross structures. These structures emanate from a complicated amalgamation of microscopic shell-structure and collective dynamics and show that such dependencies are not always amenable to phenomenological modeling. For example, for certain combinations of angular momentum and energy, two cluster orbits in the separating fragments may have a large overlap in momentum space, which substantially

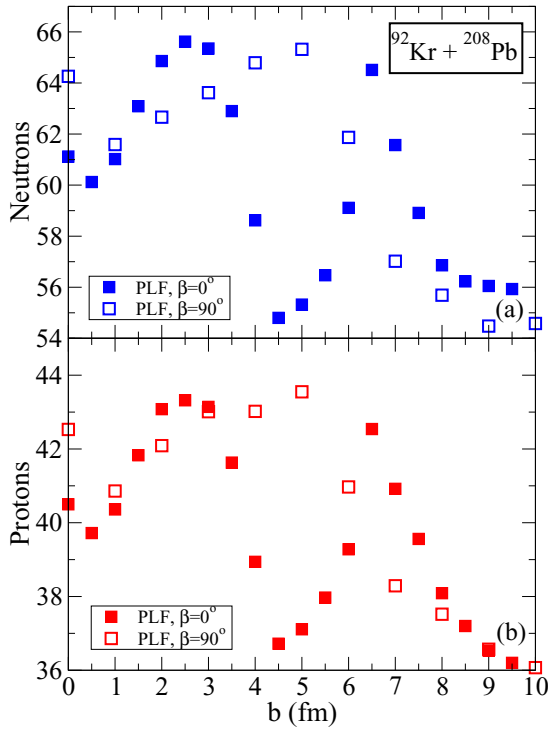

FIG. 5. (a) Neutron and (b) proton numbers of the PLF for the reaction ^{92}Kr + ^{208}Pb at $E = 8.5$ MeV/nucleon as a function of impact parameter b (fm). Angle β represents the initial orientation of the deformed ^{92}Kr nucleus with respect to the beam axis.

enhances the probability for the transfer of particles. Furthermore, they may not necessarily be indicated in experimentally observed quantities.

Dissipative aspects of a deep-inelastic reaction are often studied in terms of the dependence of energy loss on the deflection angle. The deflection function (the c.m. scattering angle versus the initial orbital angular momentum $L_{\text{c.m.}}$) is related to the differential cross section and the dependence of the final kinetic energy of the fragments, versus the scattering angle. The contour plot of constant cross section in the deflection angle and kinetic energy plane is called the Wilczynski plot [94]. In Fig. 6 we show the deflection function plotted as a function of the initial orbital angular momentum. For reference we also show the pure Rutherford scattering deflection angle (green curve). As we see for head-on collisions ($L_{\text{c.m.}} = 0$) and for the most peripheral collisions the deflection function approaches the Rutherford scattering limit. In the intermediate region of partial waves the balance of the attractive nuclear force and repulsive Coulomb and centrifugal forces determines the behavior. A stronger deflection due to nuclear orbiting is observed in the collisions induced by the ^{92}Kr beam. This can be interpreted as an effect of larger angular momentum in these collisions. Indeed, the partial wave corresponding to the grazing angle can be obtained using the sharp-cutoff model to be 518$\hbar$ for ^{78}Kr and 596$\hbar$ for ^{92}Kr.

Figure 7 shows the total kinetic energy (TKE) versus scattering angle. Fully damped collisions produce fragments with the same TKE in both reactions, with a strong orbiting (spanning all angles) characteristic of deep-inelastic collisions.

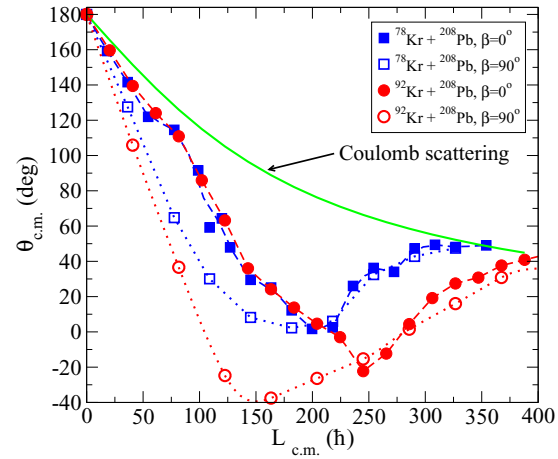

FIG. 6. The deflection function for the reactions ^{78}Kr + ^{208}Pb and ^{92}Kr + ^{208}Pb at $E = 8.5$ MeV/nucleon. Angle β represents the initial orientation of the deformed Kr nuclei with respect to the beam axis. As a reference we also show the Rutherford scattering deflection angle (green curve).

Figures 6 and 7 demonstrate the strong correlation of the energy loss with the deflection angle and accordingly with the impact parameter. These results show that TDHF calculations reproduce many of the main features of deep-inelastic collision phenomena. In the language of models these are related to the phenomena of orbiting incorporating friction. Finally, we should mention that the TDHF results yield single curves which should be compared with the most probable experimental energy-angle correlation, the maximum of the contours.

B. N/Z equilibration

The influence of isospin flow during strongly damped heavy-ion reactions is usually discussed in terms of the N/Z asymmetry of the target and projectile. In the current study the N/Z values for ^{78}Kr and ^{92}Kr are 1.16 and 1.55, respectively. The N/Z value for ^{208}Pb is 1.54. This implies

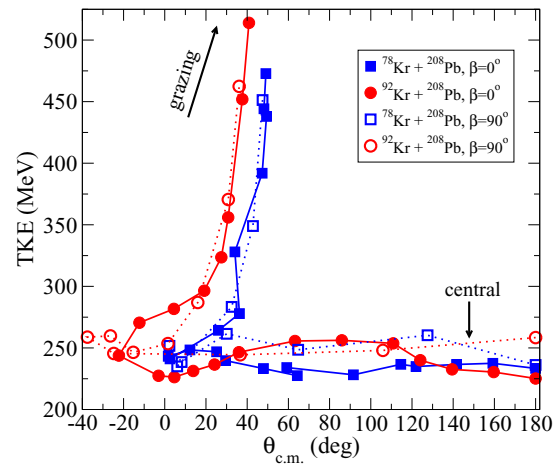

FIG. 7. The final kinetic energy versus the scattering angle for the reactions ^{78}Kr + ^{208}Pb and ^{92}Kr + ^{208}Pb at $E = 8.5$ MeV/nucleon. Angle β represents the initial orientation of the deformed Kr nuclei with respect to the beam axis.

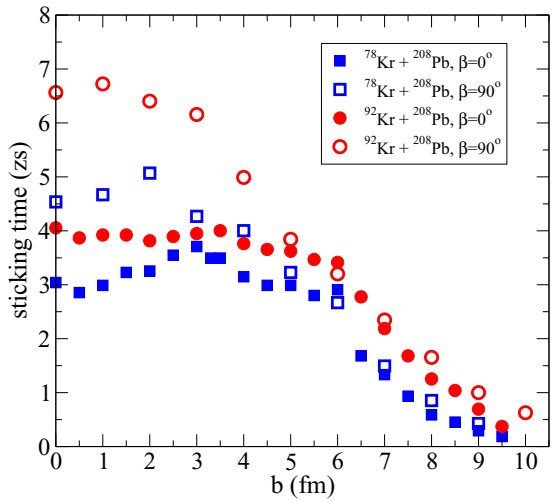

FIG. 8. The sticking time as a function of impact parameter for $^{78}\mathrm{Kr} + ^{208}\mathrm{Pb}$ and $^{92}\mathrm{Kr} + ^{208}\mathrm{Pb}$ at $E = 8.5$ MeV/nucleon. Angle β represents the initial orientation of the deformed Kr nuclei with respect to the beam axis.

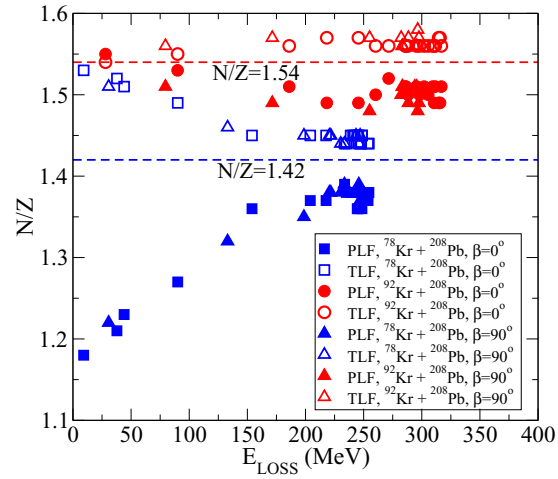

FIG. 9. The N/Z values for PLF and TLF as a function of E_{loss} for $^{78}\mathrm{Kr} + ^{208}\mathrm{Pb}$ and $^{92}\mathrm{Kr} + ^{208}\mathrm{Pb}$ at $E = 8.5$ MeV/nucleon. Angle β represents the initial orientation of the deformed Kr nuclei with respect to the beam axis. The horizontal lines represent the N/Z values for the compound system for the two reactions.

that the $^{92}\mathrm{Kr} + ^{208}\mathrm{Pb}$ reaction is a nearly N/Z symmetric collision. The N/Z values for the compound systems for $^{78}\mathrm{Kr} + ^{208}\mathrm{Pb}$ and $^{92}\mathrm{Kr} + ^{208}\mathrm{Pb}$ are 1.42 and 1.54, respectively. For an N/Z asymmetric system the fragments emerging from a deep-inelastic collision should have their average somewhere between the N/Z values of the target and the projectile, depending on the degree of equilibration. Naturally, the amount of equilibration depends on the energy and impact parameter, which determine the amount of time the system spends in a di-nuclear configuration. In Fig. 8 we plot the sticking time (time spent from the initial contact to final separation) as a function of impact parameter and initial orientation of Kr. First, we observe the obvious, namely, the most peripheral collisions are fast and have the least time for equilibration, whereas the central impact parameters allow for much longer equilibration times. We also observe that for central collisions the dependence of sticking time on the orientation of the Kr nuclei is evident, with perpendicular orientation resulting in much longer sticking times. It is very interesting to compare these sticking times with the final (N, Z) content of the fragments depicted in Figs. 4 and 5. For example, the structures observed in the $^{92}\mathrm{Kr} + ^{208}\mathrm{Pb}$ collision for the $\beta = 0^\circ$ orientation around the $b = 4.5$ fm region cannot simply be explained by the sticking time which is relatively smooth in this region. This suggests that for such collisions while the sticking time plays a certain role in determining the reaction products shell effects are still very important. This is one of the reasons why modeling of these reactions based on general macroscopic assumptions may not always be appropriate.

The measure of N/Z equilibration during the reaction is shown in Fig. 9 in terms of the N/Z values of the PLF and targetlike fragment (TLF). As expected, we observe that for peripheral collisions, the PLF and TLF N/Z values are close to the projectile and target values, respectively. For the $^{78}\mathrm{Kr} + ^{208}\mathrm{Pb}$ reaction, these values are quite different, and thus a large degree of charge equilibration is observed in more damped collisions, producing fragments with N/Z values close (but not equal) to the N/Z of the compound system. Indeed, the PLF and TLF N/Z values in $^{78}\mathrm{Kr} + ^{208}\mathrm{Pb}$ fully damped collisions are $\sim$1.38 and $\sim$1.44, respectively, while the compound system has $N/Z \simeq 1.42$.

In contrast, for the $^{92}\mathrm{Kr} + ^{208}\mathrm{Pb}$ system, we observe only small deviations around the initial N/Z values of the fragments as the system is already close to equilibrium as far as the isospin degree of freedom is concerned. Looking into details, it is interesting to note that for strongly damped collisions the N/Z values in the fragments become slightly more asymmetric than in the entrance channel ($\sim$1.56 for the PLF and $\sim$1.50 for the TLF).

The fact that N/Z values of the fragments are not exactly equal, even in fully damped collisions, is not a signature for being out of isospin equilibrium [16]. Indeed, the thermodynamic equation of state indicates that the fragments should approach a common chemical potential (in our case strongly affected by symmetry energy) rather than a common composition. In fact, the N/Z value provides only an approximate proxy for the chemical potential which depends on variations in internal energy, density, and ground-state binding energies.

Nevertheless, the neutron and proton composition dependence with the contact time can be use to estimate the charge equilibration time. Charge equilibration is often achieved within about 1 zs, as shown by earlier TDHF calculations [95]. Figure 10 shows the evolution of $(N - Z)/A$ as a function of contact time T. An equilibration time $\tau \sim 0.5$ zs is obtained from the fit $(N - Z)/A = \alpha + \beta \exp(-T/\tau)$. Recently, Jedele *et al.* [16] obtained a slightly faster equilibration time of $\sim$0.3 zs from experimental data at Fermi energy. The fact that the TDHF method gives a charge equilibration time of the same order indicates that it incorporates the essential physics to describe this process. This also indicates that the charge equilibration mechanisms ought to be similar at different energy regimes.

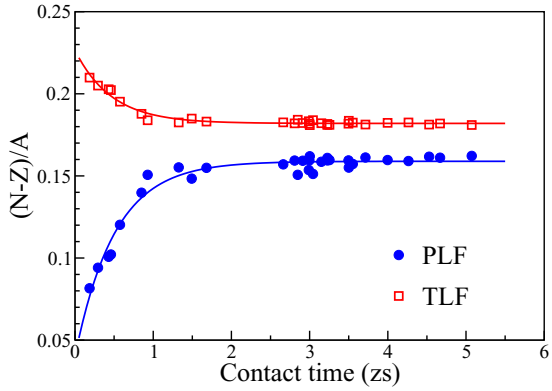

FIG. 10. The $(N-Z)/A$ values of the primary PLF (solid circles) and TLF (open squares) formed in $^{78}\mathrm{Kr}+^{208}\mathrm{Pb}$ at $E=8.5$ MeV/nucleon are plotted as a function of the contact time between the collision partners. The solid lines show fits to the TDHF results (see text).

C. From primary fragments to cold residues

If we neglect the fast nucleon evaporation occurring before the last time iteration of the TDHF calculation, the PLF and TLF fragments calculated by the TDHF method correspond to primary fragments. The absence of quantal decay (other than evaporation of single-particle wave functions) and transitions prevents us from dynamically calculating the secondary and further fragments. It is expected that the primary fragments will undergo various processes to approach the β-stability line in time [19]. However, assuming that it is statistical in character, the deexcitation process can be calculated with programs like GEMINI [96,97] provided realistic inputs can be obtained. In addition to the mass and charge of the PLF we calculate the excitation energy of each primary fragment (discussed in the next section) as well as the angular momentum "loss" (i.e., transfer from initial orbital angular momentum to intrinsic angular momentum of the fragments). Assuming a division of remaining angular momentum in proportion to PLF mass one has all the ingredients to employ the GEMINI code to calculate the deexcitation process (other parameters set to default values). The methods described in Refs. [19,98] were applied to obtain the centroids for the Z and N distributions of post-evaporative projectilelike fragments.

Similar to previous studies [19], in Fig. 11 we show the evolution of the centroids of the nuclide distributions in the N-Z plane for different energy-loss bins for the $^{78}\mathrm{Kr}+^{208}\mathrm{Pb}$ system. The initial ^{78}Kr position is marked with the symbol $\times$. The open symbols indicate the primary fragments, while the solid symbols show the fragments after deexcitation. We also show the line corresponding to the compound nucleus N/Z value of 1.42, and the β-stability line. As we also observed in Fig. 9 the primary fragments corresponding to strongly damped collisions approach N/Z values close to the compound nucleus line. Also shown in Fig. 11 are the deexcited fragments (solid circles) calculated with the GEMINI deexcitation code. We see that the deexcited fragments congregate on and around the β-stability line. As expected the

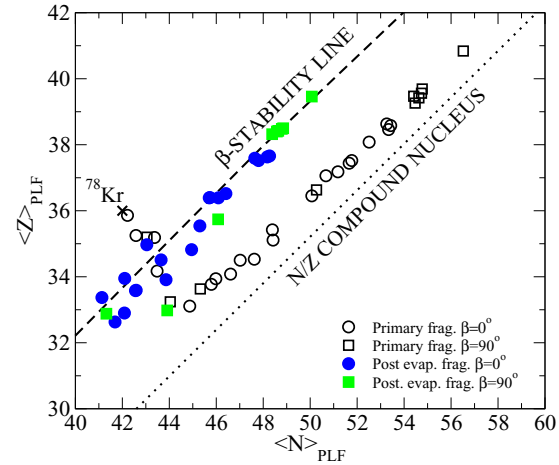

FIG. 11. The distribution of PLF neutron and proton numbers plotted in the N-Z plane for the $^{78}\mathrm{Kr}+^{208}\mathrm{Pb}$ system at $E=8.5$ MeV/nucleon. Angle β represents the initial orientation of the deformed Kr nuclei with respect to the beam axis. The initial ^{78}Kr position is marked with $\times$. The open symbols indicate the primary fragments, while the solid symbols show the fragments after deexcitation.

primary fragments with higher excitation originating from the strongly damped collisions have a better chance for deexciting to the β-stability line. In Fig. 12 we show the evolution of the centroids of the nuclide distributions in the N-Z plane for different energy-loss bins for the $^{92}\mathrm{Kr}+^{208}\mathrm{Pb}$ system. The initial ^{92}Kr position is marked with the symbol $\times$. Again, the open symbols indicate the primary fragments, while the solid symbols show the fragments after deexcitation. The β-stability line and the line corresponding to the compound nucleus N/Z

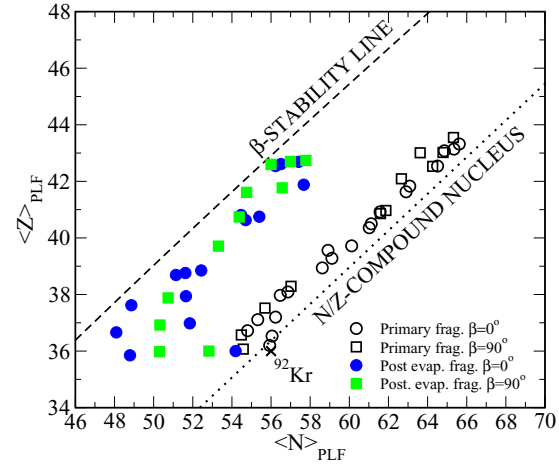

FIG. 12. The distribution of PLF neutron and proton numbers plotted in the N-Z plane for the $^{92}\mathrm{Kr}+^{208}\mathrm{Pb}$ system at $E=8.5$ MeV/nucleon. Angle β represents the initial orientation of the deformed Kr nuclei with respect to the beam axis. The initial ^{92}Kr position is marked with $\times$. The open symbols indicate the primary fragments, while the solid symbols show the fragments after deexcitation.

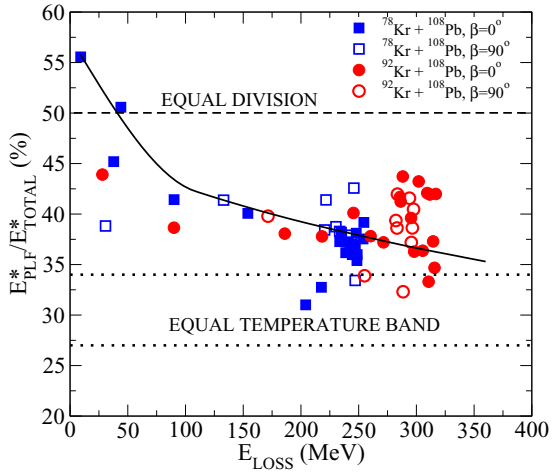

FIG. 13. Percent of total excitation energy carried by the PLF as a function of $E_{\rm loss}$. Angle β represents the initial orientation of the deformed Kr nuclei with respect to the beam axis. The dashed horizontal line marks equal sharing of excitation energy. The region between the dotted lines indicates the full thermalization limit.

value of 1.54 are also shown. Compared to the $^{78}\mathrm{Kr} + ^{208}\mathrm{Pb}$ system the primary fragments produced in $^{92}\mathrm{Kr} + ^{208}\mathrm{Pb}$ are more neutron rich, meaning that they are farther away from the β-stability line. Also, one can notice a similar decay chain length for the excited primary fragments in the two reactions. As a result, the post-evaporative fragments in $^{92}\mathrm{Kr} + ^{208}\mathrm{Pb}$ are more neutron rich; that is, they are slightly farther from the β-stability line in comparison with the $^{78}\mathrm{Kr} + ^{208}\mathrm{Pb}$ system.

D. Excitation energies

One of the most interesting aspects of strongly damped collisions is the partial transformation of the initial available energy into various forms of excitation via dissipative (heat) or nondissipative processes, such as deformation and spin of the fragments [3]. The excitation energy division between the PLF and TLF is intimately related to N/Z equilibration, the degree to which thermal equilibrium is reached, and relaxation times. In this section, we discuss the excitation properties of the produced primary fragments using the method described in Sec. II B.

In Fig. 13 we show the percent fraction of the excitation energy carried by the PLF as a function of $E_{\rm loss}$ for all the systems studied. The solid line is drawn by hand to show the general trend of the results. Also shown by a dashed line is the equal sharing of the excitation energy as well as the band between the two dashed lines corresponding to the case for equal temperature thermal equilibrium for PLF and TLF for which the sharing of the excitation energy $E^*_{\rm PLF}/E^*_{\rm total} = A_{\rm PLF}/A_{\rm total}$ [40]. The vertical width of the band reflects the distribution of $A_{\rm PLF}$. We observe that for low $E_{\rm loss}$ values the partition of the excitation energy is closer to the equal sharing line. However, as the energy loss increases, the repartition of excitation energy gets closest to the thermal equilibrium limit but rarely reaches there. It is satisfactory to see that these fully microscopic calculations, with no parameter adjusted on reaction properties, are able to affirm previous experimental observations [34,36].

IV. SUMMARY AND DISCUSSION

The TDHF method in full three dimensions is employed to calculate deep-inelastic reactions of $^{78}\mathrm{Kr} + ^{208}\mathrm{Pb}$ and $^{92}\mathrm{Kr} + ^{208}\mathrm{Pb}$ systems. The impact parameter and energy-loss dependence of relevant observables are calculated. In addition, the density-constrained TDHF method is used to compute excitation energies of the primary fragments. The statistical deexcitation code GEMINI is utilized to examine the final reaction products.

We find a smooth dependence of the energy loss, $E_{\rm loss}$, on the impact parameter for both systems. However, the transfer properties for low $E_{\rm loss}$ values are very different for the two systems but become similar in the higher $E_{\rm loss}$ regime. The impact parameter dependence of transfer shows more structure emanating from shell effects and orientation of the deformed projectile.

A charge equilibration process is observed when the nuclei have an initial N/Z asymmetry, with an increased N/Z equilibration as the energy damping is increased. However, even fully damped collisions usually do not lead to identical N/Z values in the fragment. This is because the N/Z content of the fragment is only an approximate proxy for the chemical potential. Nevertheless, the evolution of the N/Z values of the fragments as a function of contact time can be used to investigate the charge equilibration process. Experimentally, contact times are not a direct observable but can be reconstructed by comparison with theoretical predictions of the fragment properties (mass, charge, scattering angle, and kinetic energy). The present TDHF calculations indicate a mean lifetime of charge equilibration of $\sim$0.5 zs, of the same order as the mean lifetime obtained from experimental data at Fermi energies.

The fully microscopic TDHF theory has shown itself to be rich in nuclear phenomena and continues to stimulate our understanding of nuclear dynamics. The time-dependent mean-field studies seem to show that the dynamic evolution builds up correlations that are not present in the static theory. While there is evidence that one-body dissipation can properly account for the transport phenomena seen in these reactions, further experiments are needed to test this conclusion.

ACKNOWLEDGMENTS

This work has been supported by the U.S. Department of Energy under Grant No. DE-SC0013847, by the Australian Research Council Grants No. FT120100760 and No. DP160101254, and by the National Natural Science Foundation of China under Grant No. 11575044 and the China Scholarship Council (File No. 201606095006).

[1] W. U. Schröder and J. R. Huizenga, Damped heavy-ion collisions, Annu. Rev. Nucl. Part. Sci. **27**, 465 (1977).

[2] L. G. Moretto and R. P. Schmitt, Deep inelastic reactions: A probe of the collective properties of nuclear matter, Rep. Prog. Phys. **44**, 533 (1981).

[3] J. Tõke and W. U. Schröder, Excitation energy division in dissipative heavy-ion collisions, Annu. Rev. Nucl. Part. Sci. **42**, 401 (1992).

[4] C. H. Dasso, G. Pollarolo, and A. Winther, Systematics of Isotope Production with Radioactive Beams, Phys. Rev. Lett. **73**, 1907 (1994).

[5] P. Danielewicz, R. Lacey, and W. G. Lynch, Determination of the equation of state of dense matter, Science **298**, 1592 (2002).

[6] Bao-An Li, Àngels Ramos, G. Verde, and I. Vidaña, Topical issue on nuclear symmetry energy, Eur. Phys. J. A **50**, 1 (2014).

[7] M. B. Tsang, Z. Chajecki, D. Coupland, P. Danielewicz, F. Famiano, R. Hodges, M. Kilburn, F. Lu, W. G. Lynch, J. Winkelbauer, M. Youngs, and Y. X. Zhang, Constraints on the density dependence of the symmetry energy from heavy-ion collisions, Prog. Part. Nucl. Phys. **66**, 400 (2011).

[8] C. J. Horowitz, E. F. Brown, Y. Kim, W. G. Lynch, R. Michaels, A. Ono, J. Piekarewicz, M. B. Tsang, and H. H. Wolter, A way forward in the study of the symmetry energy: Experiment, theory, and observation, J. Phys. G **41**, 093001 (2014).

[9] Bao-An Li, Lie-Wen Chen, and Che Ming Ko, Recent progress and new challenges in isospin physics with heavy-ion reactions, Phys. Rep. **464**, 113 (2008).

[10] X. Roca-Maza, M. Centelles, X. Viñas, and M. Warda, Neutron Skin of ^{208}Pb, Nuclear Symmetry Energy, and the Parity Radius Experiment, Phys. Rev. Lett. **106**, 252501 (2011).

[11] Wei-Chia Chen and J. Piekarewicz, Searching for isovector signatures in the neutron-rich oxygen and calcium isotopes, Phys. Lett. B **748**, 284 (2015).

[12] M. B. Tsang, Y. Zhang, P. Danielewicz, M. Famiano, Z. Li, W. G. Lynch, and A. W. Steiner, Constraints on the Density Dependence of the Symmetry Energy, Phys. Rev. Lett. **102**, 122701 (2009).

[13] N. Chamel and P. Haensel, Physics of neutron star crusts, Living Rev. Relativ. **11**, 10 (2008).

[14] G. Shen, C. J. Horowitz, and S. Teige, New equation of state for astrophysical simulations, Phys. Rev. C **83**, 035802 (2011).

[15] M. B. Tsang, T. X. Liu, L. Shi, P. Danielewicz, C. K. Gelbke, X. D. Liu, W. G. Lynch, W. P. Tan, G. Verde, A. Wagner, H. S. Xu, W. A. Friedman, L. Beaulieu, B. Davin, R. T. de Souza, Y. Larochelle, T. Lefort, R. Yanez, V. E. Viola, R. J. Charity, and L. G. Sobotka, Isospin Diffusion and the Nuclear Symmetry Energy in Heavy Ion Reactions, Phys. Rev. Lett. **92**, 062701 (2004).

[16] A. Jedele, A. B. McIntosh, K. Hagel, M. Huang, L. Heilborn, Z. Kohley, L. W. May, E. McCleskey, M. Youngs, A. Zarrella, and S. J. Yennello, Characterizing Neutron–Proton Equilibration in Nuclear Reactions with Subzeptosecond Resolution, Phys. Rev. Lett. **118**, 062501 (2017).

[17] R. Planeta, S. H. Zhou, K. Kwiatkowski, W. G. Wilson, V. E. Viola, H. Breuer, D. Benton, F. Khazaie, R. J. McDonald, A. C. Mignerey, A. Weston-Dawkes, R. T. de Souza, J. R. Huizenga, and W. U. Schröder, *N/Z* equilibration in damped collisions induced by $E/A = 8.5$ MeV ^{58}Ni and ^{64}Ni on ^{238}U, Phys. Rev. C **38**, 195 (1988).

[18] R. T. de Souza, W. U. Schröder, J. R. Huizenga, R. Planeta, K. Kwiatkowski, V. E. Viola, and H. Breuer, Evolution of mass and charge asymmetry in damped heavy-ion reactions, Phys. Rev. C **37**, 1783 (1988).

[19] R. Płaneta, K. Kwiatkowski, S. H. Zhou, V. E. Viola, H. Breuer, M. A. McMahan, W. Kehoe, and A. C. Mignerey, Nucleon exchange properties of the $E/A = 8.5$ MeV ^{74}Ge + ^{165}Ho reaction, Phys. Rev. C **41**, 942 (1990).

[20] A. B. Balantekin, J. Carlson, D. J. Dean, G. M. Fuller, R. J. Furnstahl, M. Hjorth-Jensen, R. V. F. Janssens, Bao-An Li, W. Nazarewicz, F. M. Nunes, W. E. Ormand, S. Reddy, and B. M. Sherrill, Nuclear theory and science of the facility for rare isotope beams, Mod. Phys. Lett. A **29**, 1430010 (2014).

[21] J. Rizzo, Ph. Chomaz, and M. Colonna, A new approach to solve the Boltzmann-Langevin equation for fermionic systems, Nucl. Phys. A **806**, 40 (2008).

[22] M. Colonna, M. Di Toro, A. Guarnera, S. Maccarone, M. Zielinska-Pfabé, and H. H. Wolter, Fluctuations and dynamical instabilities in heavy-ion reactions, Nucl. Phys. A **642**, 449 (1998).

[23] M. Di Toro, V. Baran, M. Colonna, and V. Greco, Probing the nuclear symmetry energy with heavy-ion collisions, J. Phys. G **37**, 083101 (2010).

[24] C. Rizzo, V. Baran, M. Colonna, A. Corsi, and M. Di Toro, Symmetry energy effects on fusion cross sections, Phys. Rev. C **83**, 014604 (2011).

[25] Y. Zhang, D. D. S. Coupland, P. Danielewicz, Z. Li, H. Liu, F. Lu, W. G. Lynch, and M. B. Tsang, Influence of in-medium NN cross sections, symmetry potential, and impact parameter on isospin observables, Phys. Rev. C **85**, 024602 (2012).

[26] M. Colonna, Fluctuations and Symmetry Energy in Nuclear Fragmentation Dynamics, Phys. Rev. Lett. **110**, 042701 (2013).

[27] S. Ayik, B. Schürmann, and W. Nörenberg, Microscopic transport theory of heavy-ion collisions, Z. Phys. A **279**, 145 (1976).

[28] J. Randrup, Theory of transfer-induced transport in nuclear collisions, Nucl. Phys. A **327**, 490 (1979).

[29] C. B. Das, S. Das Gupta, W. G. Lynch, A. Z. Mekjian, and M. B. Tsang, The thermodynamic model for nuclear multifragmentation, Phys. Rep. **406**, 1 (2005).

[30] J. Blocki, Y. Boneh, J. R. Nix, J. Randrup, M. Robel, A. J. Sierk, and W. J. Swiatecki, One-body dissipation and super-viscidity of nuclei, Ann. Phys. **113**, 330 (1978).

[31] H. Feldmeier, Transport phenomena in dissipative heavy-ion collisions: The one-body dissipation approach, Rep. Prog. Phys. **50**, 915 (1987).

[32] D. H. E. Gross and H. Kalinowski, Friction model of heavy-ion collisions, Phys. Rep. **45**, 175 (1978).

[33] M. Baldo, A. Rapisarda, R. A. Broglia, and A. Winther, Multiparticle transfer and frictional forces in heavy ion collisions, Nucl. Phys. A **472**, 333 (1987).

[34] R. Vandenbosch, A. Lazzarini, D. Leach, D.-K. Lock, A. Ray, and A. Seamster, Nonequilibrium Excitation-Energy Division in Deeply Inelastic Collisions, Phys. Rev. Lett. **52**, 1964 (1984).

[35] J. Wilczynski and H. W. Wilschut, Partition of excitation energy in the optimum Q-value model, Phys. Rev. C **39**, 2475 (1989).

[36] T. C. Awes, R. L. Ferguson, R. Novotny, F. E. Obenshain, F. Plasil, S. Pontoppidan, V. Rauch, G. R. Young, and H. Sann, Energy Division in Damped Reactions, Phys. Rev. Lett. **52**, 251 (1984).

[37] J. Randrup, Transport of angular momentum in damped nuclear reactions, Nucl. Phys. A **383**, 468 (1982).

[38] H. Feldmeier and H. Spangenberger, Particle exchange as the dissipative mechanism in nucleus-nucleus collisions, Nucl. Phys. A **428**, 223 (1984).

[39] H. Freiesleben and J. V. Kratz, NZ-equilibration and nucleon exchange in dissipative heavy-ion collisions, Phys. Rep. **106**, 1 (1984).

[40] R. Płaneta, K. Kwiatkowski, S. H. Zhou, V. E. Viola, H. Breuer, M. A. McMahan, J. Randrup, and A. C. Mignerey, Nucleon exchange and heat partition in damped collisions, Phys. Rev. C **39**, 1197 (1989).

[41] J. S. Barrett, W. Loveland, R. Yanez, S. Zhu, A. D. Ayangeakaa, M. P. Carpenter, J. P. Greene, R. V. F. Janssens, T. Lauritsen, E. A. McCutchan, A. A. Sonzogni, C. J. Chiara, J. L. Harker, and W. B. Walters, ^{136}Xe + ^{208}Pb reaction: A test of models of multinucleon transfer reactions, Phys. Rev. C **91**, 064615 (2015).

[42] D. C. Rafferty, M. Dasgupta, D. J. Hinde, C. Simenel, E. C. Simpson, E. Williams, I. P. Carter, K. J. Cook, D. H. Luong, S. D. McNeil, K. Ramachandran, K. Vo-Phuoc, and A. Wakhle, Multinucleon transfer in ^{16,18}O, ^{19}F + ^{208}Pb reactions at energies near the fusion barrier, Phys. Rev. C **94**, 024607 (2016).

[43] W. U. Schröder and J. R. Huizenga, in *Treatise on Heavy-Ion Science*, edited by D. A. Bromley (Plenum, New York, 1984), Vol. 2, p. 115.

[44] N. Alahari, S. Ayik, R. Bougault, G. Casini, M. Chartier, A. Chbihi, M. Dasgupta, D. J. Hinde, D. Lacroix, R. Lemmon, M. Rejmund, C. Schmitt, C. Simenel, G. Verde, and the FAZIA Collaboration, Transport properties of isospin asymmetric nuclear matter, SPIRAL2 technical report, 2016 (unpublished).

[45] A. S. Umar, M. R. Strayer, D. J. Ernst, and K. R. Sandhya Devi, Mean-field theory of prompt, high-energy nucleon emission, Phys. Rev. C **30**, 1934 (1984).

[46] J. W. Negele, The mean-field theory of nuclear-structure and dynamics, Rev. Mod. Phys. **54**, 913 (1982).

[47] Cédric Simenel, Nuclear quantum many-body dynamics, Eur. Phys. J. A **48**, 152 (2012).

[48] T. Nakatsukasa, K. Matsuyanagi, M. Matsuo, and K. Yabana, Time-dependent density-functional description of nuclear dynamics, Rev. Mod. Phys. **88**, 045004 (2016).

[49] K. T. R. Davies, K. R. Sandhya Devi, and M. R. Strayer, Fusion behavior in time-dependent Hartree-Fock calculations of ^{86}Kr + ^{139}La and ^{84}Kr + ^{209}Bi collisions, Phys. Rev. C **24**, 2576 (1981).

[50] K. T. R. Davies, K. R. S. Devi, S. E. Koonin, and M. R. Strayer, in *Treatise on Heavy-Ion Science*, edited by D. A. Bromley (Plenum, New York, 1985), Vol. 3, p. 3.

[51] A. S. Umar, M. R. Strayer, and P.-G. Reinhard, Resolution of the Fusion Window Anomaly in Heavy-Ion Collisions, Phys. Rev. Lett. **56**, 2793 (1986).

[52] A. S. Umar, M. R. Strayer, P.-G. Reinhard, K. T. R. Davies, and S.-J. Lee, Spin-orbit force in time-dependent Hartree-Fock calculations of heavy-ion collisions, Phys. Rev. C **40**, 706 (1989).

[53] S.-J. Lee, A. S. Umar, K. T. R. Davies, M. R. Strayer, and P.-G. Reinhard, Enhanced dissipation in new mean-field studies of strongly damped collisions, Phys. Lett. B **196**, 419 (1987).

[54] K. Washiyama, D. Lacroix, and S. Ayik, One-body energy dissipation in fusion reactions from mean-field theory, Phys. Rev. C **79**, 024609 (2009).

[55] M. Tohyama and A. S. Umar, Quadrupole resonances in unstable oxygen isotopes in time-dependent density-matrix formalism, Phys. Lett. B **549**, 72 (2002).

[56] Cédric Simenel, Particle-Number Fluctuations and Correlations in Transfer Reactions Obtained Using the Balian-Vénéroni Variational Principle, Phys. Rev. Lett. **106**, 112502 (2011).

[57] D. Lacroix and S. Ayik, Stochastic quantum dynamics beyond mean field, Eur. Phys. J. A **50**, 95 (2014).

[58] Y. Iwata, T. Otsuka, J. A. Maruhn, and N. Itagaki, Suppression of Charge Equilibration Leading to the Synthesis of Exotic Nuclei, Phys. Rev. Lett. **104**, 252501 (2010).

[59] K. Sekizawa and K. Yabana, Time-dependent Hartree-Fock calculations for multinucleon transfer processes in ^{40,48}Ca + ^{124}Sn, ^{40}Ca + ^{208}Pb, and ^{58}Ni + ^{208}Pb reactions, Phys. Rev. C **88**, 014614 (2013).

[60] C. Simenel and B. Avez, Time-dependent Hartree-Fock description of heavy ions fusion, Int. J. Mod. Phys. E **17**, 31 (2008).

[61] A. S. Umar, V. E. Oberacker, and J. A. Maruhn, Neutron transfer dynamics and doorway to fusion in time-dependent Hartree-Fock theory, Eur. Phys. J. A **37**, 245 (2008).

[62] D. Bourgin, C. Simenel, S. Courtin, and F. Haas, Microscopic study of ^{40}Ca + ^{58,64}Ni fusion reactions, Phys. Rev. C **93**, 034604 (2016).

[63] K. Vo-Phuoc, C. Simenel, and E. C. Simpson, Dynamical effects in fusion with exotic nuclei, Phys. Rev. C **94**, 024612 (2016).

[64] J. F. Liang, J. M. Allmond, C. J. Gross, P. E. Mueller, D. Shapira, R. L. Varner, M. Dasgupta, D. J. Hinde, C. Simenel, E. Williams, K. Vo-Phuoc, M. L. Brown, I. P. Carter, M. Evers, D. H. Luong, T. Ebadi, and A. Wakhle, Examining the role of transfer coupling in sub-barrier fusion of ^{46,50}Ti + ^{124}Sn, Phys. Rev. C **94**, 024616 (2016).

[65] K. Godbey, A. S. Umar, and C. Simenel, Dependence of fusion on isospin dynamics, Phys. Rev. C **95**, 011601(R) (2017).

[66] A. Wakhle, C. Simenel, D. J. Hinde, M. Dasgupta, M. Evers, D. H. Luong, R. du Rietz, and E. Williams, Interplay Between Quantum Shells and Orientation in Quasifission, Phys. Rev. Lett. **113**, 182502 (2014).

[67] V. E. Oberacker, A. S. Umar, and C. Simenel, Dissipative dynamics in quasifission, Phys. Rev. C **90**, 054605 (2014).

[68] A. S. Umar, V. E. Oberacker, and C. Simenel, Shape evolution and collective dynamics of quasifission in the time-dependent Hartree-Fock approach, Phys. Rev. C **92**, 024621 (2015).

[69] K. Hammerton, Z. Kohley, D. J. Hinde, M. Dasgupta, A. Wakhle, E. Williams, V. E. Oberacker, A. S. Umar, I. P. Carter, K. J. Cook, J. Greene, D. Y. Jeung, D. H. Luong, S. D. McNeil, C. S. Palshetkar, D. C. Rafferty, C. Simenel, and K. Stiefel, Reduced quasifission competition in fusion reactions forming neutron-rich heavy elements, Phys. Rev. C **91**, 041602(R) (2015).

[70] A. S. Umar, V. E. Oberacker, and C. Simenel, Fusion and quasifission dynamics in the reactions ^{48}Ca + ^{249}Bk and ^{50}Ti + ^{249}Bk using a time-dependent Hartree-Fock approach, Phys. Rev. C **94**, 024605 (2016).

[71] K. Sekizawa and K. Yabana, Time-dependent Hartree-Fock calculations for multinucleon transfer and quasifission processes in the ^{64}Ni + ^{238}U reaction, Phys. Rev. C **93**, 054616 (2016).

[72] A. S. Umar, V. E. Oberacker, J. A. Maruhn, and P.-G. Reinhard, Microscopic calculation of precompound excitation energies for heavy-ion collisions, Phys. Rev. C **80**, 041601 (2009).

[73] V. E. Oberacker, A. S. Umar, J. A. Maruhn, and P.-G. Reinhard, Microscopic study of the ^{132,124}Sn + ^{96}Zr reactions: Dynamic excitation energy, energy-dependent heavy-ion potential, and capture cross section, Phys. Rev. C **82**, 034603 (2010).

[74] P.-G. Reinhard, A. S. Umar, K. T. R. Davies, M. R. Strayer, and S.-J. Lee, Dissipation and forces in time-dependent Hartree-Fock calculations, Phys. Rev. C **37**, 1026 (1988).
[75] A. S. Umar, M. R. Strayer, J. S. Wu, D. J. Dean, and M. C. Güçlü, Nuclear Hartree-Fock calculations with splines, Phys. Rev. C **44**, 2512 (1991).
[76] Ka-Hae Kim, T. Otsuka, and P. Bonche, Three-dimensional TDHF calculations for reactions of unstable nuclei, J. Phys. G **23**, 1267 (1997).
[77] J. A. Maruhn, P. G. Reinhard, P. D. Stevenson, J. R. Stone, and M. R. Strayer, Dipole giant resonances in deformed heavy nuclei, Phys. Rev. C **71**, 064328 (2005).
[78] T. Nakatsukasa and K. Yabana, Linear response theory in the continuum for deformed nuclei: Green's function vs time-dependent Hartree-Fock with the absorbing boundary condition, Phys. Rev. C **71**, 024301 (2005).
[79] A. S. Umar and V. E. Oberacker, Three-dimensional unrestricted time-dependent Hartree-Fock fusion calculations using the full Skyrme interaction, Phys. Rev. C **73**, 054607 (2006).
[80] L. Guo, J. A. Maruhn, P.-G. Reinhard, and Y. Hashimoto, Conservation properties in the time-dependent Hartree Fock theory, Phys. Rev. C **77**, 041301 (2008).
[81] J. A. Maruhn, P.-G. Reinhard, P. D. Stevenson, and A. S. Umar, The TDHF code Sky3D, Comput. Phys. Commun. **185**, 2195 (2014).
[82] E. Chabanat, P. Bonche, P. Haensel, J. Meyer, and R. Schaeffer, A Skyrme parametrization from subnuclear to neutron star densities. Part II: Nuclei far from stabilities, Nucl. Phys. A **635**, 231 (1998).
[83] P. Klüpfel, P.-G. Reinhard, T. J. Bürvenich, and J. A. Maruhn, Variations on a theme by Skyrme: A systematic study of adjustments of model parameters, Phys. Rev. C **79**, 034310 (2009).
[84] M. Kortelainen, T. Lesinski, J. More, W. Nazarewicz, J. Sarich, N. Schunck, M. V. Stoitsov, and S. Wild, Nuclear energy density optimization, Phys. Rev. C **82**, 024313 (2010).
[85] K. Washiyama, S. Ayik, and D. Lacroix, Mass dispersion in transfer reactions with a stochastic mean-field theory, Phys. Rev. C **80**, 031602 (2009).
[86] R. Balian and M. Vénéroni, Time-Dependent Variational Principle for Predicting the Expectation Value of an Observable, Phys. Rev. Lett. **47**, 1353 (1981).
[87] P. Klein, J. V. Kratz, M. K. Gober, H. P. Zimmermann, W. Brüchle, W. Reisdorf, and M. Schädel, Excitation energy division in ^{51}V + ^{197}Au collisions at and near the barrier, Z. Phys. A **357**, 193 (1997).
[88] Ph. Chomaz, N. V. Giai, and S. Stringari, Lifetimes of monopole resonances in time-dependent Hartree-Fock theory, Phys. Lett. B **189**, 375 (1987).
[89] B. Avez and C. Simenel, Structure and direct decay of giant monopole resonances, Eur. Phys. J. A **49**, 76 (2013).
[90] R. Y. Cusson, P.-G. Reinhard, M. R. Strayer, J. A. Maruhn, and W. Greiner, Density as a constraint and the separation of internal excitation energy in TDHF, Z. Phys. A **320**, 475 (1985).
[91] A. S. Umar and V. E. Oberacker, Heavy-ion interaction potential deduced from density-constrained time-dependent Hartree-Fock calculation, Phys. Rev. C **74**, 021601 (2006).
[92] K. Sekizawa and K. Yabana, Particle-number projection method in time-dependent Hartree-Fock theory: Properties of reaction products, Phys. Rev. C **90**, 064614 (2014).
[93] C. Bottcher, M. R. Strayer, A. S. Umar, and P.-G. Reinhard, Damped relaxation techniques to calculate relativistic bound-states, Phys. Rev. A **40**, 4182 (1989).
[94] J. Wilczyński, Optimum Q-value in multinucleon transfer reactions, Phys. Lett. B **47**, 124 (1973).
[95] C. Simenel, D. J. Hinde, R. du Rietz, M. Dasgupta, M. Evers, C. J. Lin, D. H. Luong, and A. Wakhle, Influence of entrance-channel magicity and isospin on quasi-fission, Phys. Lett. B **710**, 607 (2012).
[96] R. Charity, GEMINI: A code to simulate the decay of a compound nucleus by a series of binary decays, IAEA Technical Report INDC(NDS)-0530, 2008 (unpublished).
[97] R. J. Charity, Systematic description of evaporation spectra for light and heavy compound nuclei, Phys. Rev. C **82**, 014610 (2010).
[98] H. Breuer, N. R. Yoder, A. C. Mignerey, V. E. Viola, K. Kwiatkowski, and K. L. Wolf, The analysis of simultaneous mass and charge data from damped heavy-ion reactions, Nucl. Instrum. Methods Phys. Res. **204**, 419 (1983).